S-nitrosylation of CYR61 protein reduces triple-negative breast cancer metastasis ability

Lee Jia (jiali@fzu.edu.cn)
Fuzhou University https://orcid.org/0000-0003-2963-7331
Yusheng Lu
Minjiang University
Sudan He
Fuzhou University
Huanzhang Xie
Minjiang University
Chunlian Zhong
Minjiang University
Xingtian Yang
Fuzhou University
Suhong Yu
Fuzhou University
Shu Lian
Fuzhou University
Yumei Li
Fuzhou University
Guoxing Lin
Fuzhou University
Chen Zhang
Minjiang University

Research

Keywords: S-nitrosylation, CYR61 protein, Breast cancer, Cancer metastasis, Nitric oxide

Posted Date: October 8th, 2020

DOI: https://doi.org/10.21203/rs.3.rs-86057/v1

Abstract

Background

Triple-negative breast cancer (TNBC) is the most difficult cancer to be treated. TNBC expresses high level of matricellular cysteine-rich protein CYR61/CCN1 that plays a key role in producing cancer metastases and is an important target for metastasis chemoprevention. Nitric oxide (NO) can covalently bind to the thiol group of cysteines (termed S-nitrosylation) resulting in regulation of the targeted protein functions.

Methods

Protein S-nitrosylation were detected by biotin-switch assay and western blotting assay. CYR61 protein S-nitrosylated sites and 3D structure were determined by mass spectrometry and MODELLER software. Adhesion assay, cell morphology assay, wound healing assay and transwell invasion assay were used to evaluate effects of CYR61 S-nitrosylation on the cell metastatic ability. In vivo metastasis activity of CYR61 S-nitrosylation were tested by intravenous injection and mammary xenograft implantation mouse metastatic models.

Results

S-nitrosylation by GSNO of CYR61 reached a plateau quickly and was confirmed by spectroscopic analysis and biotin-switch assay. Mass-spectrometry proteomic analysis revealed that S-nitrosylation predominantly occurred at Cys100, Cys117, Cys229 and Cys239, resulting in CYR61 structure relaxed and unstable evidenced by protein structure modeling. S-nitrosylation of MDA-MB-231 cells, their CYR61-overexpressed and CYR61–silenced counterparts significantly attenuated the metastatic ability of these cells, including their ability of adhesion, mobility, invasion, and interplay with platelets, and made the adhered cells unattached. The attenuation in metastatic ability proportionally increased with the degree of S-nitrosylation to CYR61 naturally-expressed or genetically-manipulated cells, and was demonstrated in mice, where, S-nitrosylation of these cell lines not only inhibited their acute seeding to lungs after an intravenous injection, but also inhibited the late development of these cells into the metastatic nodes after mammary xenograft implantation. Furthermore, orthotopically-implanted MDA-MB-231 developed mammary tumors and later lung metastasis; whereas, the same cells with S-nitrosylation developed no tumor and metastasis at all.

Conclusion

we present the first evidence that S-nitrosylation of CYR61 can significantly inhibit metastatic aggressiveness of the TNBC MDA-MB-231 cells. This conceptual creative study opens a new avenue to prevent the most aggressive TNBC from metastases by S-nitrosylation to CYR61.

Background

Breast cancer is the most frequently diagnosed cancer and the leading cause of cancer death in females worldwide, accounting for 23% of the total new cancer cases and 14% of the total cancer deaths. Triple negative breast cancer (TNBC) lacked the expression of estrogen receptors (ER), progesterone receptors (PgR) and HER2 accounts for approximately 15% of all breast cancer diagnosis and is responsible for a great share of mortality [1], few therapeutic strategies are proved efficient against TNBC once it metastasizes.

The human cysteine-rich protein 61 (CYR61/CCN1) belongs to the CCN family of genes, and plays a key role in cancer cell activities, including proliferation, migration, adhesion, invasion, and differentiation, and survival. This secreted matricellular protein is a member of CCN family, consists of 381 amino acids, including 38 conserved cysteine [2]. CYR61 is highly expressed in breast cancer, in particular, in the TNBC cell line MDA-MB-231. The high expression of CYR61 in MDA-MB-231 cells is also demonstrated by our recent pharmacoproteomic analysis [3, 4].

Nitric oxide (NO) serves as an endogenous signaling molecule, binds to cysteine thiol side-chains in multiple proteins to form S-nitrosothiols (RSNOs). The covalent addition of an NO group to the thiol group of cysteine is termed S-nitrosylation, which represents an important cellular regulatory mechanism in primarily cardiovascular system [5–11]. NO reacts with reducing sulfhydryl group of the sulfhydryl compounds to produce S-nitrosothiols such as S-nitrosoglutathione (GSNO) and S-nitrosocaptopril [12, 13], which are more stable than NO.

Post-translational modification of proteins plays a critical role in the living body. The biological process complicates the structure, optimizes the function and elaborates the regulation of proteins to gain their specificity. S-nitrosylation of proteins has been shown to confer NO-like biological activities and to regulate protein functions. S-nitrosylation is precisely targeted with respect to both protein substrates and specific subject to modification under pathophysiological conditions, and is precisely regulated in space and time by nitrosylating and denitrosylating mechanisms that play the regulatory role in myriad signal transduction cascades, including hemoglobin [14, 15], G protein-coupled receptors [16], and many others.

Inspired by our previous successes in S-nitrosylation of various molecules, which indeed alter functions of the tested molecules [13–15], we here examine our hypothesis that S-nitrosylation of CYR61 (CYR61-SNO) may change CYR61 functionality, resulting in attenuation of character, and reduce the metastatic aggressiveness of TNBC MDA-MB-231. The study may further reveal the pathophysiological relevance of CYR61, and discover a new path to overcome CYR61-related TNBC metastasis.

Materials And Methods

Materials

SiRNA-CYR61 and negative SiRNA-control were purchased from Sangon Biotech (Shanghai). Pierce S-Nitrosylation western blot kit, immobilized anti-TMT Resin and TMT elution buffer were purchased from

Thermo scientific. Anti-CYR61 was from Abcam. The recombinant plasmid of pcDNA3.1-CYR61 was constructed by our lab.

Cell lines and culture

MDA-MB-231 cells were obtained from American Type Culture Collection (ATCC, Manassas, VA), and were incubated with Leibovitz's L-15 medium (Catalog No. 30-2008) containing 10% fetal bovine serum, 100 U/ml penicillin and 100 μg/ml streptomycin at 37°C in a free gas exchange with atmospheric air. Human pulmonary microvascular endothelial cells (HPMEC) were purchased from Promocell, and were cultured in ECM with 10% fetal bovine serum, 100 U/ml penicillin and 100 μg/ml streptomycin at 37°C in 5% CO_2 atmosphere.

Construction of Si-CYR61 and OE-CYR61 MDA-MB-231 cells

SiRNA oligos and recombinant plasmid pcDNA3.1-CYR61 were constructed by our lab. SiRNA sequence: 5'-AACAUCAGUGCACAUGTAUUG-3'. CYR61 cDNA cloning primer: sense, 5'-taa aag ctt atg agc tcc cgc atc gcc ag-3' and antisense, 5'-ccc ctc gag tta gtc cct aaa ttt gtg aat gtc-3'. Transient transfection of MDA-MB-231 cells with siRNA oligos (100 pmol) and recombinant plasmid pcDNA3.1-CYR61 (4 μg/well) was carried out using Lipofectamine®3000 Transfection Reagent Protocol (life technologies), according to the manufacturer's instructions. Nontargeting siRNA and empty pcDNA3.1 vector were served as negative controls, respectively. These cells were harvested 24 h after transfection and used for further analysis.

Biotin switch assay

Biotin-switch assay was performed to verify protein S-nitrosylation [17, 18]. In brief, cell lysates were diluted with HENS buffer (Pierce) and then treated with methyl methanethiol-sulfonate (MMTS) (Pierce) in a final concentration of 20 mM at room temperature. After 30 min, MMTS was removed by passing the samples through a spin column three times. The samples were then incubated with ascorbic acid (Pierce) to release the NO from the thiol group, and were subsequently biotinylated by incubating with biotin-TMT (Pierce). The biotinylated proteins were then precipitated by incubating the samples with 50 μl of neutravidin-agarose (Pierce). The neutravidin-agarose was then pelleted and washed 5 times using HENS buffer. The biotinylated proteins were eluted by TMT-elution buffer (Pierce).

Spectroscopic analysis

MDA-MB-231 s were lysed by RIPA with 1% PMSF, and the cell's protein concentrations were measured by BCA. Lysates were treated with 1- and 10-fold acidified NO_2^- for 20 min, respectively, and were then scanned with UV-visible spectroscopy.

S-nitrosylation optimization

The degree of S-nitrosylation (S-nitrosylated protein/total protein) was used to evaluate the trans-nitrosylation reaction between GSNO and proteins. Briefly, MDA-MB-231 s and OE-CYR61 MDA-MB-231 s were cultured with GSNO (10 and 30 μM) for different times and were lysed in HENS buffer. Biotin switch assay was used to label S-nitrosylated protein with -TMT. The total protein amount was measured by BCA

assay. The S-nitrosylated proteins were collected by the affinity resin column and quantitatively measured by the BCA assay.

Western blotting assay

Western blotting assay was performed to evaluate protein expression levels as we described previously [19]. Briefly, MDA-MB-231 cells cultured in the present of GSNO (0, 10 and 30 μM) were lysed by RIPA with 1% PMSF. Antibodies used for western blotting analysis included CYR61 antibody and TMT. Immunodetection of electrophoresis-resolved proteins was accomplished using the enhanced chemiluminescence based on the standard protocols. The signal intensity was quantified with a quantitative digital imaging system (Quantity One, Bio-Rad).

S-nitrosylation verification

MDA-MB-231 s were cultured with GSNO, GSH, and GSNO plus DTT (all 30 μM), respectively. Biotin switch assay and western blotting assay were performed to detect protein S-nitrosylation. The S-nitrosylated protein was collected by the affinity resin column. Western blotting assay was performed to detect CYR61 S-nitrosylation.

Determination of S-nitrosylated Cys in CYR61

S-nitrosation of the recombinant CYR61 was determined liquid chromatography with tandem mass spectrometry (LC-MS/MS) analysis [20, 21]. Recombinant CYR61 protein (PeproTech) was incubated with GSNO (30 μM) for 30 min at room temperature. Proteins were trypsinized and desalted by using a C18 desalting column, followed by protein lyophilization. The lyophilized powder was dissolved in solution A (100% water, 0.1% formic acid) and injected into a C18 Nano-Trap column (2 cm × 75 μm, 3 μm) and separated by an analytical column (15 cm × 150 μm, 1.9 μm), using a linear gradient elution as listed in **Supplementary Table 1**. The separated peptides were analyzed by Q Exactive HF-X mass spectrometer (Thermo Fisher), with ion source of Nanospray Flex™ (ESI), spray voltage of 2.3 kV and ion transport capillary temperature of 320 °C. Full scan range from *m/z* 350 to 1500 with resolution of 60000 (at *m/z* 200), an automatic gain control (AGC) target value was 3×10^6 and a maximum ion injection time was 20 ms. The top 40 precursors of the highest abundant in the full scan were selected and fragmented by higher energy collisional dissociation (HCD) and analyzed by the MS/MS, where the resolution was 15000 (at *m/z* 200), the AGC target value was 1×10^5, the maximum ion injection time was 45 ms, the normalized collision energy of 27%, the intensity threshold of 2.2×10^4, and the dynamic exclusion parameter of 20 s. The resulting spectra from each fraction were searched by the search engines: Proteome Discoverer 2.2 (PD 2.2, Thermo). The search parameters were set as follows: mass tolerance for precursor ion was 10 ppm and mass tolerance for product ion was 0.02 Da. Carbamidomethyl was specified in PD 2.2 as fixed modifications. Oxidation of methionine and acetylation of the N-terminus were specified in PD 2.2 as variable modifications. The maximum of 2 missed cleavage sites was allowed. The identified protein contains at least 1 unique peptide with FDR no more than 1.0%.

In vitro **cytotoxicity studies**

Cell viability was assessed using MTT assay as we described previously [19, 22, 23]. MDA-MB-231 cells were trypsinized and seeded on 96-well plates at 8×10^3 cells/well. After 24-h culture and adhesion, GSNO (0, 10, 50, 100, 200 and 500 μM) was added to the cell culture for another 12-h incubation. Then, MTT (5 mg/ml, 100-μl per well) was added and incubated for 4 hours. The MTT solution was aspirated and replaced with 100 μl/well dimethyl sulfoxide solution (DMSO). After 30-min mixing, the plates were measured at wavelength 570 nm using an infinite M200 Pro microplate reader (Tecan, Switzerland). Each experiment was performed in triplicate.

Heterotypic cell adhesion assay

Quantification of MDA-MB-231 cell adhesion to endothelial cells was carried out as we described previously [3, 23, 24]. Briefly, HPMECs (10^5 each well) were grown to confluence on 24-well plates. Then TNF-α (final concentration 10 ng/ml) was used to activate HPMECs for 4 hours. GSNO (0, 10 and 30 μM) and Rhodamine 123-labeled MDA-MB-231 cells and their genetically-transfected CYR61 cell lines were co-cultured with the HPMECs monolayers in each well for 2 hours. Non-adhered MDA-MB-231 s were removed by PBS wash. Ten random visual fields for each well were selected and photographed using a fluorescence microscope (Zeiss Axio Observer A1, Germany). Mean inhibition of adhesion for 10 visual fields was calculated by using the equation: % of control adhesion= [the number of adhered cells /the number of adhered cells in the MDA-MB-231 control group] × 100%. Each experiment was performed in triplicate.

Cell-matrix adhesion assay

To conduct a cell-matrix adhesion assay, HPMECs were replaced with gelatins, the later was used to simulate the extracellular matrix. The 24-well plate was coated with 100 μL gelatin per well and incubated for 24 hours. The gelatin-coated 24-well plates were blocked with PBS containing 1% BSA for 30 min before the adhesion assay. BSA was thoroughly removed with PBS for three times. Rhodamine 123-labeled MDA-MB-231 cells and their genetically-transfected CYR61 cell lines were cultured with GSNO (0, 10 and 30 μM) for 2 hours. Non-adhered MDA-MB-231 s were removed by PBS. Ten random visual fields for each well were selected and taken pictures using a fluorescence microscope (Zeiss Axio Observer A1, Germany). Mean inhibition of adhesion for 10 visual fields was calculated by using the equation: % of control adhesion= [the number of adhered cells /the number of adhered cells in the MDA-MB-231 control group] × 100%. Each experiment was performed in triplicate.

Wound healing assay.

Wound healing assay was performed to analyze cell migration in vitro as we described previously[25, 26]. MDA-MB-231 cells and their genetically-transfected CYR61 cell lines were seeded in 12-well plates and incubated to become confluent. Sterile tips were used to scratch the cell layers, which were subsequently washed with PBS for three times, and then cultured with 1 mL of L-15 media containing 2% FBS and different concentrations (0, 10, 30 μM) of GSNO. The cells were photographed by using a fluorescence microscope (Zeiss, Germany) at 0, 24 and 48 h. Each experiment was performed in triplicate.

Cell invasion assay.

Matrigel is the trade name for a gelatinous protein mixture secreted by Engelbreth-Holm-Swarm (EHS) mouse sarcoma cells. The transwell invasion assay was conducted as we described previously [25]. The upper chambers of the transwells (24-well, 8 μm pore size) were treated with Matrigel (Becton Dickinson, Waltham, MA, USA) and air-dried. The lower chambers were filled with 750 μL of media containing 20% FBS. MDA-MB-231 cells and their genetically-transfected CYR61 cell lines were seeded at the density of 3×10^4 per well (200 μL) on the upper chambers in L-15 media containing GSNO (0, 10 and 30 μM) and 1% FBS. After 24 hours, the cells that had invaded through the Matrigel membrane were stained with crystal violet, and photographed by using a fluorescence microscope (Zeiss, Germany) (five random fields). Each experiment was performed in triplicate.

Platelet adhesion assay

Platelet adhesion assay was performed as we described previously [27]. Freshly anticoagulated whole blood was centrifuged at 200 × g for 10 minutes, and the supernatant (platelet rich plasma, PRP) was collected followed by centrifugation at 1500 × g for 15 minutes, Platelets were precipitated, and the supernatant was platelet-poor plasma (PPP). Platelets were resuspended and adjusted to the range of $1–3 \times 10^6$/μL by diluting with autologous PPP. MDA-MB-231 cells and their genetically-transfected CYR61 cell lines were grown to confluence on 12-well plates, respectively. Then, CFSE-labeled platelets and GSNO (0, 10 and 30 μM) were co-cultured with the MDA-MB-231 s monolayers in each well, followed by addition of ADP (20 μM) to stimulate the platelet activation. After 1-hour incubation at 37 °C, non-adhered platelets and cells were removed by three times of PBS wash. Ten random visual fields for each well were selected and photographed by using the Leica TCS SP8 confocal microscope. The mean inhibition of adhesion for 20 visual fields was calculated by using the equation: % of control adhesion = [the number of adhered cells / the number of adhered cells in the MDA-MB-231 control group] × 100%. Each experiment was performed in triplicate.

Cell morphology assay

MDA-MB-231 cells (2.5×10^4) were cultured with GSNO (30 μM) in a 35-mm cell culture dish (NEST, GBD-35-20). Morphology change of the cells was analyzed by using a time-lapse photography program of the leica TCS SP8 confocal microscope.

Mice

BALB/C nude mice (20 ± 2 g, 4–6 weeks old) were purchased from Shanghai SLAC Laboratory and maintained under clean conditions. Mice were housed in clean, pathogen-free room in an environment with controlled temperature (26 ℃), humidity (55%), and a 12-hour light/dark cycle, and maintained with free access to pellet food and water in microinsulator cages. All animals used in the investigation were handled in accordance with the Guide for the Care and Use of Laboratory Animals (National Research Council, 1996), and approved by the institutional animal care and use committee of Fuzhou University.

MDA-MB-231 lung metastasis experiment

The nude mice were divided into nine groups (n = 8 per group). The CFSE-labeled MDA-MB-231 cells and their genetically-transfected CYR61 cell lines were pre-treated with GSNO (0, 10 and 30 μM) for 30 min and washed 3 times in PBS. The cells (5×10^6) were resuspended in 200 μl of PBS, and injected into the lateral tail vein of mice. Four hours after the injections, the nude mice were sacrificed and their lungs were excised, and frozen sectioned, and photographed by using the leica TCS SP8 confocal microscope.

In vivo **tumor pulmonary metastasis study**

The nude mice were divided into treatment groups and control group randomly (n = 8 per group). MAD-MB-231 s were treated with GSNO (0, 10 and 30 μM) for 30 min and washed 3 times in PBS. The cells (5×10^6) were resuspended in 200 μl of PBS, and injected into the lateral tail vein of the mice. Ten weeks after the injection, the nude mice were sacrificed and their lungs were excised. The number of surface lung tumor nodules was counted. The lungs were then paraffin-embedded and stained with hematoxylin and eosin (H&E) for histological examination.

In vivo **tumor xenograft study**

The nude mice were divided into three groups (8–10 per group). MDA-MB-231 cells treated with or without GSNO were resuspended in 50 μl of PBS, respectively, and injected into mammary fat pad (group1: MDA-MB-231 s and GSNO-treated MDA-MB-231 cells were injected orthotopically into the different mammary fat pad of the same immunodeficient mouse; group 2: MDA-MB-231 s were injected orthotopically into mammary fat pad; group 3: GSNO-treated MDA-MB-231 cells were injected orthotopically into mammary fat pad). Two weeks after the injections, the tumor growth was observed. Six weeks after the injections, the nude mice were sacrificed and their lungs were excised and photographed.

Statistical analysis

Data are presented as the mean ± standard error of the mean (SEM), or mean ± standard deviations (SD). Statistical analysis was performed using the student's t-test and one-way analysis of variance. A P-value less than 0.05 was considered statistically significant.

Results

Quantitative and qualitative analysis of CYR61 S-nitrosylation

As shown in Fig. 1, MDA-MB-231 cells and their genetically-manipulated cell lines, which were either transfected with CYR61-related recombinant plasmid pcDNA3.1-CYR61 to overexpress cysteine-rich protein 61 (OE-CYR61 MDA-MB-231 cells), or with siRNA oligos (Si-CYR61 MDA-MB-231 cells) to reduce

CYR61 expression, were exposed to GSNO at 0, 10 and 30 μM for different times in order to determine 1) the optimal exposure time for intramolecular transfer of NO from GSNO to thiols of CYR61 and the whole cells; 2) if the trans-S-nitrosylation reaction is GSNO concentration-dependent.

The iodo TMT labeling reagent was added to the whole cell protein to transfer S-nitrosylated molecules (RSNO) to RS-TMT. The total protein and its RSNO portion were measured by the BCA protein assay and the biotin-switch assay, respectively. After quantifying the S-TMT group by using the biotin-switch assay, the RS-TMT protein was obtained from the affinity resin column following the buffer elution, and quantitatively determined by the BCA protein assay. Among the RS-TMT protein, the amount of CYR61 was further determined by the CYR61 Western Blotting assay, and was assumed to be equivalent to that of CYR61-SNO.

To demonstrate that this nitrosylation reaction modifies proteins of MDA-MB-231 cells, we treated the tested cell lysis with excess acidified NO_2^-. The resultant solutions were scanned with UV-visible spectroscopy, which showed absorption maxima at 350 and 540 nm, indicative of nitrosation and S-nitrosylation products formed [11]. The optical absorption density increased proportionally with the increasing quantities of NO_2^- (Fig. 2A).

To find out the optimal time for intermolecular transfer of NO from GSNO to cysteine rich protein and the whole cell protein, we incubated MDA-MB-231 and OE-CYR61 MDA-MB-231 cell lines with GSNO of low and high concentrations (10 and 30 μM) for different times, and then determined the ratio of S-nitrosylated protein to the total cell protein for optimizing S-nitrosylation conditions. As shown in Fig. 2B, the intermolecular transfer of NO from GSNO to the tested cell lines reached the maximum at 30 min of cell incubation with GSNO. Longer incubation of the cell lines with GSNO did not produce more the trans-S-nitrosylation reaction, probably because the limited source of GSNO has been exhausted and converted to GSSG and RSNO, we thus used 30 min as the optimal reaction time for the intermolecular transfer of NO from GSNO to the tested cell lines throughout the present study. Interestingly, there was trace amount of S-nitrosylated products detected by the biotin-switch assay at 0 min before addition of GSNO to the reaction system (Fig. 2B). The trace amount of CYR61-SNO was also shown in Fig. 2D when no GSNO was added to the reaction system. The noise RSNO detected by the assay may result from the endogenous RSNO existing in the cells and cell medium, or from the TMT-SR eluted from the affinity resin column. Nonetheless, production of CYR61-SNO was GSNO concentration-dependent (Fig. 2D). Figure 2C showed all the S-nitrosylated proteins detected by the biotin-switch assay in MDA-MB-231 cells treated with 30 μM of GSNO for 30 min. DTT abolished the trans-S-nitrosylation reaction between GSNO and thiol-rich protein (the far-right lane of Fig. 2C), and the result is consistent with what we reported that DTT antagonized vasorelaxation induced by S-nitrosylated cysteine (CysNO) [28]. Included in the same sample, we also detected CYR61 protein by using the Western Blotting assay specific for CYR61. The result showed that CYR61 amount was proportional to the total RSNO amount in the cells. In addition, the stain intensity of Western Blotting for CYR61 was directly related to GSNO concentrations of 10 and 30 μM (Fig. 2D), confirming the formation of CYR61-SNO. We therefore named MAD-MB-231 and its alike

samples treated with 0, 10 and 30 μM of GSNO as the control, low and high CYR61-SNO for clear presentation of the present study.

To further explore if the specific S-nitrosylation occurred at CYR61, we incubated the three cell lines expressing low, medium, and high levels of CYR61 with 30 μM of GSNO for 30 min along with their non-targeting siRNA and empty pcDNA3.1 vector as the controls, and measured the CYR61-SNO produced from each of the cell lines. As shown in Fig. 2E, Si-CYR61 MDA-MB-231 cells produced significantly lesser CYR61-SNO than MDA-MB-231 cells (47% vs. 100%). By contrast, OE-CYR61 MDA-MB-231 cells produced significantly more CYR61-SNO than MDA-MB-231 (236% vs. 100%), reflecting the specific trans-S-nitrosylation mainly from GSNO to CYR61.

To confirm that there was no cytotoxic effect with 30 μM of GSNO that would otherwise kill the tested cells directly, we conducted the cell viability study by using a broad range of GSNO from 10 μM- 500 mM. As shown in Fig. 2F, we could not reach the IC50 value (the concentration causing 50% growth inhibition of the cells) GSNO, confirming that the effects of GSNO on cell activities observed in the present study result directly from its biological S-nitrosylation efficacy, not from any apoptotic or cytotoxic effect.

S-nitrosylation of cysteine residues in CYR61 and thereafter

To identify which cysteine residues were specifically S-nitrosylated, we incubated the recombinant CYR61 protein with GSNO (30 μM) for 30 min, and determined the site S-nitrosylation reaction by using LC-MS/MS based proteomic analysis [23]. As shown in Fig. 3A, cysteine residues at 100, 117, 229 and 239 were found to be S-nitrosylated, respectively, and the S-nitrosylated sites in the primary structure of CYR61 were red-highlighted in Fig. 3B. The four residues may represent the important functions of CYR61 as we showed with other Cys-containing proteins before [11, 14]. MODELLER software was then used for comparative modeling of CYR61 protein 3D structure before and after S-nitrosylation. Since the 3D structure of CYR61 protein is unknown, we extracted various pieces of the similar short structural fragments from the known protein library for comparative docking analysis[29]. Figure 3C shows the 3D structure of CYR61 protein subunit 1 (Glu96-Asp164) and subunit 2 (Lys228 -Gly273). Surprisingly, after S-nitrosylation, MODELLER could not build a stable structure of the two subunits, suggesting that S-nitrosylation make CYR61 structure relaxed and less stable.

S-nitrosylation down-regulates CYR61 adhesion ability

CYR61 plays an important role in cellular adhesion. To test if S-nitrosylation of the cysteine-rich molecule could change the adhesion ability of MDA-MB-231, we incubated MDA-MB-231, OE-CYR61-MDA-MB-231, and Si-CYR61-MDA-MB-231, respectively, with gelatin (Fig. 4A **and Supplementary Fig. 1**) or HPMECs (Fig. 4B **and Supplementary Fig. 2**) in the presence and absence of GSNO, and measured the change in adhesion ability of these cell lines.

As shown in Fig. 4A and compared with the untreated normal MDA-MB-231 control, S-nitrosylation significantly reduced adhesion of MDA-MB-231 cells to gelatin by 70% and 60% (low and high CYR61-

SNO), respectively. OE-CYR61 MDA-MB-231 adhered more to gelatin than the untreated MDA-MB-231 control (130%). After S-nitrosylation, the aggressive adhesion ability of OE-CYR61 MDA-MB-231 cells significantly reduced to 58% (high CYR61-SNO) in comparison with the untreated OE-CYR61 MDA-MB-231 cells, which was 72% reduction from the untreated control. In comparison with the untreated MDA-MB-231 control, Si-CYR61 MDA-MB-231 adhered less to gelatin (88%), and S-nitrosylation significantly reduced the adhesion ability of Si-CYR61 MDA-MB-231 cells to 63% (high CYR61-SNO) in comparison with the untreated Si-CYR61 MDA-MB-231 cells, which was 25% reduction from the untreated Si-CYR61 MDA-MB-231 control.

As shown in Fig. 4B and compared with the untreated MDA-MB-231 control, S-nitrosylation significantly reduced heterotypic adhesion of MDA-MB-231 cells to HPMECs to 73% and 52% (low and high CYR61-SNO), respectively. OE-CYR61 MDA-MB-231 adhered more to HPMECs than the untreated MDA-MB-231 control (129%). After S-nitrosylation, the aggressive adhesion ability of OE-CYR61 MDA-MB-231 cells significantly reduced to 75% and 49% (low and high CYR61-SNO), respectively, in comparison with the untreated OE-CYR61 MDA-MB-231 cells, which was 80% reduction from the untreated control. In comparison with the untreated MDA-MB-231 control, Si-CYR61 MDA-MB-231 adhered less to HPMECs (85%), and S-nitrosylation significantly reduced the adhesion ability of Si-CYR61 MDA-MB-231 cells to 55% (high CYR61-SNO) in comparison with the untreated Si-CYR61 MDA-MB-231 cells, which was 30% reduction from the untreated Si-CYR61 MDA-MB-231 control.

CYR61 S-nitrosylation inhibits migration and invasion ability of MDA-MB-231

Migration and invasion are the key steps of the breast cancer metastatic cascade. To examine if CYR61 S-nitrosylation could attenuate the aggressive metastatic ability of MDA-MB-231, we further tested the effect of CYR61 S-nitrosylation on cell motility (Fig. 4C-D). After 48 h incubation of the three cell lines with low and high levels of GSNO, the ability of the three cell lines to migrate to heal the scratch wound was significantly attenuated: the average migration distance of the MDA-MB-231 control was 252 nm; the MDA-MB-231 of low CYR61-SNO, 204 nm; and the MDA-MB-231 of high CYR61-SNO, 153 nm. Overexpression of CYR61 significantly enhanced the migration ability of the cells: the average migration distance of the OE-CYR61 MDA-MB-231 control was 304 nm; the OE-CYR61 MDA-MB-231 of low CYR61-SNO, 255 nm; and the OE-cry61 MDA-MB-231 of high CYR61-SNO, 161 nm. By contrast, CYR61 knockdown significantly alleviated the migration ability of the cells: the average migration distance of the Si-CYR61 MDA-MB-231 control was 220 nm; the Si-CYR61 MDA-MB-231 of low CYR61-SNO, 174 nm; and the Si-cry61 MDA-MB-231 of high CYR61-SNO, 153 nm. Si-CYR61 MDA-MB-231 migration distance was shortened from 220 nm, 174 nm to 153 nm, respectively. CYR61 overexpression increased migration distance and CYR61 knockdown reduced. In general, compared with MDA-MB-231 cells, the migration ability of OE-CYR61 MDA-MB-231 was relatively strong, and that of Si-CYR61 MDA-MB-231 was relatively weak. The % inhibition by CYR61 S-nitrosylation of migration ability was thus more significant in OE-CYR61 MDA-MB-231 than in Si-CYR61 MDA-MB-231 (Fig. 4C-D).

CYR61 S-nitrosylation reduced the invasion ability of the aggressive MDA-MB-231 cells. Overexpressed CYR61 enhanced the invasion ability of the transfected cells as evidenced by that more OE-CYR61 MDA-MB-231 cells passed through the transwell membrane micropores than the Si-CYR61 MDA-MB-231 cells. On the other hand, the degree of invasion reduction by the CYR61 S-nitrosylation was more significant in OE-CYR61 MDA-MB-231 cells than in Si-CYR61 MDA-MB-231 cells as shown in Fig. 4E-F. For example, for MDA-MB-231 cells, the invasion ability was reduced to 47% (low CYR61-SNO) and 24% (high CYR61-SNO) from the control, respectively. The invasion ability of OE-CYR61 MDA-MB-231 cells was reduced to 80% (low CYR61-SNO) and 21% (high CYR61-SNO), a fall of 125% from the OE-CYR61 MDA-MB-231 control. The invasion ability of Si-CYR61 MDA-MB-231 cells were changed by S-nitrosylation as well, but to a lesser degree in comparison with the overexpressed CYR61 cells because the former have lesser CYR61 available to be S-nitrosylated than the latter.

CYR61 S-nitrosylation inhibits adhesion between MDA-MB-231 and platelet and changes the cell morphology

Interplay between cancer cells and platelets often results in the so-called tumor cell-induced platelet aggregation (TCIPA) [30], which enhances the metastatic ability of cancer cells. Oppositely, GSNO inhibits aggregation of platelets[31]. We here explored the possibility that CYR61 S-nitrosylation could inhibit interplay between platelets and MDA-MB-231. We first grew MDA-MB-231 and its CYR61-transfected cell lines on the 24-well plate to > 80% confluence, and then we added GSNO and the ADP-activated platelets that were labelled with CFSE (carboxyfluorescein diacetate succinimidyl ester) to the plates for 30-min incubation. After 1-hour incubation, we washed out the unattached CFSE-labelled platelets, and quantitated those platelets attached to the cancer cells. As shown in Fig. 5, the ADP-activated platelets adhered to the cells. In comparison with MDA-MB-231 cells, OE-CYR61 MDA-MB-231 increased, but Si-CYR61 MDA-MB-231 decreased their adhesion with platelets, indicating the key role of CYR61 in the biological adhesion. CYR61 S-nitrosylation attenuated the adhesion, and the attenuation was dependent on the degree of CYR61 S-nitrosylation (Fig. 5A-B). As a result, the reduction in the adhesion was more significant in OE-CYR61 MDA-MB-231 cells, and less significant in Si-CYR61 MDA-MB-231 cells. The upper panel of Fig. 5A showed the CFSE-labeled platelets adhered to these cell lines. The middle panel showed the MDA-MB-231 and their transfected cells under bright fields (BF) of fluorescence microscopy, and the lower panel showed the interplay between the platelets and the MDA-MB-231, as well as their transfected cells after merging the upper and middle images. The above data demonstrated the important role of CYR61 S-nitrosylation in attenuating the interplay between platelets and cancer cells.

To determine if the non-toxic concentration of GSNO (30 μM) could change the morphology of MDA-MB-231, we watched the cell behaves carefully under confocal microscopy focusing on the same spot of MDA-MB-231 cells. The observation revealed separation effect of S-nitrosylation against adhesion ability of CYR61 per se (Fig. 5C). GSNO gradually changed the cell body from spindle to more round shape (see the arrows). More interestingly, the originally adhered cells became separated from each other after GSNO treatment (see the square), suggesting that S-nitrosylation change the adhesion/invasion characters of MDA-MB-231 conferred by CYR61.

CYR61 S-nitrosylation reduced mouse lung metastasis by MDA-MB-231

To test if the in vitro inhibition by CYR61 S-nitrosylation of metastatic behaves of MDA-MB-231 cells could be reproduced in vivo, we cultured enough amounts of these cell lines, and incubated them with GSNO for 30 min and removed GSNO completely before tail injection of the treated cells to BALB/C nude mice. Four hours after the cell injections, we examined the acute adhesion and accumulation of the three cell lines in mouse lungs. As shown in Fig. 6A-B, OE-CYR61 MDA-MB-231 cells adhered more, but Si-CYR61 MDA-MB-231 cells adhered less to mouse lungs in comparison with MDA-MB-231 cells. Treatment of the cell lines with GSNO significantly weakened the metastatic aggressiveness of the cells with the CYR61-overexpressed cells being affected most. We left the same batch of the mice alive for examining the subacute formation of the tumor nodes in the mouse lungs 4 weeks after cell injections. As shown in Fig. 6C-D, 30-min GSNO treatment significantly reduced the number of tumor nodes induced by MDA-MB-231 cells in a GSNO-concentration dependent manner. Both microscopic examination for micrometastatic foci and HE staining for tumor section (Fig. 6D) further confirmed that, once CYR61 protein was S-nitrosylated, the metastatic aggressiveness of MDA-MB-231 cells could be significantly attenuated.

To further test our hypothesis that S-nitrosylation of CYR61 may attenuate the metastasis aggressiveness of NTBC MDA-MB-231 cells, both the GSNO-treated (30 μM, 30 min) and untreated MDA-MB-231 cells from the same batch were injected orthotopically into the different mammary fat pad of the same immunodeficient mouse. After 2 weeks of the implantation, the untreated MDA-MB-231 cells grew aggressively in the mammary fat pad (left side) and reached an average tumor diameter of 108 ± 23 mm (n = 8) (Fig. 6E). Whereas, the same cell population treated with GSNO grow smaller tumor of 36 ± 18 mm in the right pad (Fig. 6F). Furthermore, the untreated MDA-MB-231 cells were more metastatic to the lungs from the orthotopic site 6 weeks after the primary tumor resection and the same cells treated with GSNO produced no lung metastasis at all, recapitulating the phenotypes observed with the tail vein metastasis assay. The in vivo data suggest that S-nitrosylation of CYR61 attenuate TNBC metastasis ability (Fig. 6G).

Discussion

The present study demonstrates that, for the first time, S-nitrosylation of the cysteine-rich CYR61 protein leads to attenuation of the in vitro adhesion/invasion ability of the TNBC MDA-MB-231 cells (Fig. 3–5), and their in vivo metastatic potential in the circulating cancer cell model and the mammary orthotopically-implanted metastatic model (Fig. 6). S-nitrosylation of CYR61 impaired the extravasation of the circulating MDA-MB-231 cells to the lung during the first 4 hours after tail vein injection (Fig. 6A-B), and significantly inhibited cancer metastasis induced by the circulating cancer cells to lungs after 10-week observation (Fig. 6).

Overexpression of the matricellular protein CYR61 was associated with more aggressive adhesion, migration and motility of MDA-MB-231 cells in comparison with their non-transfected MDA-MB-231 cells.

Whereas, silencing of CYR61 decreased the adhesion, migration and motility of the cells (Fig. 3–5), indicating the importance of CYR61 as a culprit in inducing cancer metastasis. The matricellular protein CYR61 contains unusually high cysteine residue content (10% or 38 in total), and is exquisitely sensitive to a wide range of microenvironmental perturbations. Its transmembrane conserved cysteine can be easily modified by the S-nitrosylation and the present proteomic analysis (Fig. 3) reveals that the S-nitrosylation site occurred primarily at cysteine residues 100, 117, 229 and 239 of CYR61, resulting in relaxed CYR61 and its less stability. The result is further supported by the fact that after S-nitrosylation, MDA-MB-231 cells became unattached (Fig. 5C). Indeed, incubation of the CYR61-overexpressed MDA-MB-231 cells with GSNO for a short period inhibited the cells' metastatic ability more significantly than MDA-MB-231 and their CYR61 silenced cell lines, and the inhibition was GSNO concentration-dependent (Fig. 4). Our findings strongly suggest the key role of the cysteine-rich CYR61 in causing cancer metastasis, and the novel strategy to antagonize the relevant metastasis by S-nitrosylation of CYR61.

Once trans-S-nitrosylation from GSNO to CYR61 was completed, or reached a plateau with a well-balanced RSNO/ protein stoichiometry, the S-nitrosylation of CYR61 could be maintained in equilibrium for at least 24 h as shown in Fig. 2A. S-nitrosylation confers the cells with NO-like biological activities, in particular, against platelet aggregation. Platelets are considered pro-metastatic by forming a physical shield around circulating tumor cells to promote cell adhesion and prevent circulating tumor cells from attack by natural killer cells [32, 33]. As shown in Fig. 5A-B, the adhesion between platelets and the tested cell lines were significantly attenuated by S-nitrosylation, which also kept the MDA-MB-231 cells apart (Fig. 5C).

Although reactivity and functional consequences of nitrosylation could occur at a variety of nucleophilic centers in proteins, biochemical analyses show that nitrosylation with thiols is the most reactive functionality [11]. Polynitrosylation by exposing the MDA-MB-231 cellular membrane to molar excess acidified nitrite showed spectroscopic characteristic peaks at 345 nm and 540 nm (Fig. 2), indicative of nitrosation and S-nitrosylation formations, respectively [11, 14]. The specificity for S-nitrosylation reaction was also demonstrated by the biotin switch assay [34] under well-controlled conditions and with appropriate controls. The specificity for S-nitrosylated CYR61 was quantitatively determined by subtracting the CYR61 amount from the total S-nitrosylated proteins measured by the Western Blotting assay. It is important to note that CYR61 has 38 conserved cysteine residues. Thus, there is the possibility of, as yet undiscovered, distinct effects of these cysteine residues on CYR61 activity and function by nitrosylation at these cysteine residues. S-nitrosylation of these individual cysteine residues may be differentially regulated, perhaps as a result of their association with different pools of endogenous nitric oxide synthase. S-nitrosylation signaling reactions are argued to play important modulatory roles in mediating the actions of NO in health and various diseases. Nonetheless, the present novel findings demonstrate that both endogenous and exogenous S-nitrosylation of CYR61 can operate in concert to attenuate the metastatic aggressiveness of the cysteine-rich TNBC, which offer new therapeutic implications.

Conclusions

In summary, our current work elucidated the key role of CYR61 S-nitrosylation in inhibiting TNBC metastasis. We demonstrated that S-nitrosylation of CYR61 protein leads to attenuation of the in vitro adhesion/invasion ability and in vivo metastatic aggressiveness of the TNBC MDA-MB-231 cells. This conceptual creative study opens a new avenue to prevent the most aggressive TNBC from metastases by S-nitrosylation to CYR61.

Abbreviations

CYR61: Cysteine-rich protein 61; TNBC:Triple-negative breast cancer; ER:Estrogen receptors; PgR:Progesterone receptors; NO:Nitric oxide; GSNO:S-nitrosoglutathione; RSNOs:S-nitrosothiols; HPMEC:Human pulmonary microvascular endothelial cells; MMTS:Methyl methanethiol-sulfonate; AGC:Automatic gain control; HCD:Higher energy collisional dissociation; EHS:Engelbreth-Holm-Swarm; PPP:Platelet-poor plasma; PRP:Platelet rich plasma; BCA:Bicinchoninic acid; TMT:Tandem Mass Tag.

Declarations

Ethical Approval and Consent to participate

The research was approved by the institutional animal care and use committee of Fuzhou University. All animal care and experiments used in the investigation were handled in accordance with the Guide for the Care and Use of Laboratory Animals (National Research Council, 1996).

Consent for publication

If this article is accepted, we will agree to publish it and transfer the copyright to academic journals and your publishing company.

Availability of supporting data

The authors declare that all the other data supporting the findings of this study are available within the article and its additional files and from the corresponding author upon reasonable request.

Competing interests

The authors declare that they have no competing interests.

Funding

This research was supported by the National Natural Science Foundation of China (NSFC, grant numbers 81703555, 81773063, 81961138017, U1505225, 81801849 and 81502617), and the China Postdoctoral Science Foundation (grant number 2017M620268).

Authors' contributions

L.J. conceived and designed the experiments. Y.L., S.H., C.Z., X.Y., Y.L. and S.L. performed the cell experiments. S.H., C.Z., X.Y., Y.L. and S.L. performed animal experiments. H.X. performed the docking analysis. L.J., Y.L., S.H., C.Z., X.Y. and H.X. acquired and analyzed the experimental data. S.Y., H.X., C.Z. and G.L. provided essential reagents and critical comments. L.J., Y.L., S.H. and X.Y. wrote the manuscript. All authors reviewed the manuscript.

Acknowledgments

We thank members of our laboratories for their suggestions.

References

1. De Laurentiis M, Cianniello D, Caputo R, Stanzione B, Arpino G, Cinieri S, Lorusso V, De Placido S. Treatment of triple negative breast cancer (TNBC): current options and future perspectives. Cancer Treat Rev. 2010;36(Suppl 3):80–6.
2. Yang R, Chen Y, Chen D. Biological functions and role of CCN1/Cyr61 in embryogenesis and tumorigenesis in the female reproductive system (Review). Mol Med Rep. 2018;17:3–10.
3. Yu S, Yang X, Zhu Y, Xie F, Lu Y, Yu T, Yan C, Shao J, Gao Y, Mo F, et al. Systems pharmacology of mifepristone (RU486) reveals its 47 hub targets and network: comprehensive analysis and pharmacological focus on FAK-Src-Paxillin complex. Sci Rep. 2015;5:7830.
4. Yu S, Yan C, Wu W, He S, Liu M, Liu J, Yang X, Ma J, Lu Y, Jia L. RU486 Metabolite Inhibits CCN1/Cyr61 Secretion by MDA-MB-231-Endothelial Adhesion. Front Pharmacol. 2019;10:1296.
5. Hess DT, Matsumoto A, Kim SO, Marshall HE, Stamler JS. Protein S-nitrosylation: purview and parameters. Nat Rev Mol Cell Biol. 2005;6:150–66.
6. Seth D, Hess DT, Hausladen A, Wang L, Wang YJ, Stamler JS. A Multiplex Enzymatic Machinery for Cellular Protein S-nitrosylation. Mol Cell. 2018;69:451–64 e456.
7. Zhou HL, Zhang R, Anand P, Stomberski CT, Qian Z, Hausladen A, Wang L, Rhee EP, Parikh SM, Karumanchi SA, Stamler JS. Metabolic reprogramming by the S-nitroso-CoA reductase system protects against kidney injury. Nature. 2019;565:96–100.
8. Seth P, Hsieh PN, Jamal S, Wang L, Gygi SP, Jain MK, Coller J, Stamler JS. Regulation of MicroRNA Machinery and Development by Interspecies S-Nitrosylation. Cell. 2019;176:1014–25 e1012.
9. Chanda PK, Meng S, Lee J, Leung HE, Chen K, Cooke JP. Nuclear S-Nitrosylation Defines an Optimal Zone for Inducing Pluripotency. Circulation. 2019;140:1081–99.
10. Tang X, Pan L, Zhao S, Dai F, Chao M, Jiang H, Li X, Lin Z, Huang Z, Meng G, et al. SNO-MLP (S-Nitrosylation of Muscle LIM Protein) Facilitates Myocardial Hypertrophy Through TLR3 (Toll-Like Receptor 3)-Mediated RIP3 (Receptor-Interacting Protein Kinase 3) and NLRP3 (NOD-Like Receptor Pyrin Domain Containing 3) Inflammasome Activation. Circulation. 2020;141:984–1000.

11. Simon DI, Mullins ME, Jia L, Gaston B, Singel DJ, Stamler JS. Polynitrosylated proteins: characterization, bioactivity, and functional consequences. Proc Natl Acad Sci U S A. 1996;93:4736–41.
12. Zhou Y, Lin M, Wang J, Chen F, Li F, Chen W, Han L, Wang C, Chen J, Shao JW, Jia L. A novel S-nitrosocaptopril monohydrate for pulmonary arterial hypertension: H2O and -SNO intermolecular stabilization chemistry. Free Radic Biol Med. 2018;129:107–15.
13. Jia L, Young X, Guo W. Physicochemistry, pharmacokinetics, and pharmacodynamics of S-nitrosocaptopril crystals, a new nitric oxide donor. J Pharm Sci. 1999;88:981–6.
14. Jia L, Bonaventura C, Bonaventura J, Stamler JS. S-nitrosohaemoglobin: a dynamic activity of blood involved in vascular control. Nature. 1996;380:221–6.
15. Stamler JS, Jia L, Eu JP, Mcmahon TJ, Demchenko IT, Bonaventura J, Gernert K, Piantadosi CA. Blood flow regulation by S-nitrosohemoglobin in the physiological oxygen gradient. Science. 1997;276:2034–7.
16. Whalen EJ, Foster MW, Matsumoto A, Ozawa K, Violin JD, Que LG, Nelson CD, Benhar M, Keys JR, Rockman HA. Regulation of β-Adrenergic Receptor Signaling by S -Nitrosylation of G-Protein-Coupled Receptor Kinase 2. Cell. 2007;129:511–22.
17. Hess DT, Stamler JS. Editorial for “Methods for Analysis of Nitric Oxide Signalling by S-nitrosylation”. Methods. 2013;62:121–2.
18. Huang B, Chen C. Detection of protein S-nitrosation using irreversible biotinylation procedures (IBP). Free Radic Biol Med. 2010;49:447–56.
19. Lu Y, Yu T, Liang H, Wang J, Xie J, Shao J, Gao Y, Yu S, Chen S, Wang L. Nitric Oxide Inhibits Hetero-adhesion of Cancer Cells to Endothelial Cells: Restraining Circulating Tumor Cells from Initiating Metastatic Cascade. Sci Rep. 2014;4:4344.
20. Li Y, Zhang Y, Wang L, Wang P, Xue Y, Li X, Qiao X, Zhang X, Xu T, Liu G, et al. Autophagy impairment mediated by S-nitrosation of ATG4B leads to neurotoxicity in response to hyperglycemia. Autophagy. 2017;13:1145–60.
21. Ban Y, Liu Y, Li Y, Zhang Y, Xiao L, Gu Y, Chen S, Zhao B, Chen C, Wang N. S-nitrosation impairs KLF4 activity and instigates endothelial dysfunction in pulmonary arterial hypertension. Redox Biol. 2019;21:101099.
22. Wang J, Chen J, Wan L, Shao J, Lu Y, Zhu Y, Ou M, Yu S, Chen H, Jia L. Synthesis, Spectral Characterization, and In Vitro Cellular Activities of Metapristone, a Potential Cancer Metastatic Chemopreventive Agent Derived from Mifepristone (RU486). Aaps Journal. 2014;16:289–98.
23. Yu S, Yan C, Yang X, He S, Liu J, Qin C, Huang C, Lu Y, Tian Z, Jia L. Pharmacoproteomic analysis reveals that metapristone (RU486 metabolite) intervenes E-cadherin and vimentin to realize cancer metastasis chemoprevention. Sci Rep. 2016;6:22388.
24. Wan L, Dong H, Xu H, Ma J, Zhu Y, Lu Y, Wang J, Zhang T, Li T, Xie J, et al. Aspirin, lysine, mifepristone and doxycycline combined can effectively and safely prevent and treat cancer metastasis: prevent seeds from gemmating on soil. Oncotarget. 2015;6:35157–72.

25. Zhou J, Yang J, Pang Y, Yang X, Yu S, Jia L. Bioactivity-guided fast screen and identification of cancer metastasis chemopreventive components from raw extracts of Murraya exotica. Journal of Pharmaceutical Biomedical Analysis. 2015;107:341–5.
26. Jiang Z, Pang Y, Yu X, Zhou S, Qian J, Zheng N, Dong H, Shi Q, Kuo M, Jia L. The paradigm-shifting idea and its practice: from traditional abortion Chinese medicine Murraya paniculata to safe and effective cancer metastatic chemopreventives. Oncotarget. 2016;7:21699–712.
27. Lu Y, Lian S, Ye Y, Yu T, Liang H, Cheng Y, Xie J, Zhu Y, Xie X, Yu S, et al. S-Nitrosocaptopril prevents cancer metastasis in vivo by creating the hostile bloodstream microenvironment against circulating tumor cells. Pharmacol Res. 2019;139:535–49.
28. Jia L, Furchgott RF. Inhibition by sulfhydryl compounds of vascular relaxation induced by nitric oxide and endothelium-derived relaxing factor. Journal of Pharmacology Experimental Therapeutics. 1993;267:371–8.
29. Webb B, Sali A. Protein Structure Modeling with MODELLER. Methods Mol Biol. 2017;1654:39–54.
30. Erpenbeck L, Schön MP. Deadly allies: the fatal interplay between platelets and metastasizing cancer cells. Blood. 2010;115:3427–36.
31. Hogg N. Biological chemistry and clinical potential of S-nitrosothiols. Free Radical Biol Med. 2000;28:1478–86.
32. Palumbo JS, Talmage KE, Massari JV, La Jeunesse CM, Flick MJ, Kombrinck KW, Jirousková M, Degen JL. Platelets and fibrin(ogen) increase metastatic potential by impeding natural killer cell-mediated elimination of tumor cells. Blood. 2005;105:178–85.
33. Gay LJ, Feldinghabermann B. Contribution of platelets to tumour metastasis. Nat Rev Cancer. 2011;11:123–34.
34. Jaffrey SR, Erdjumentbromage H, Ferris CD, Tempst P, Snyder SH. Protein S-nitrosylation: a physiological signal for neuronal nitric oxide. Nat Cell Biol. 2001;3:193.

Figures

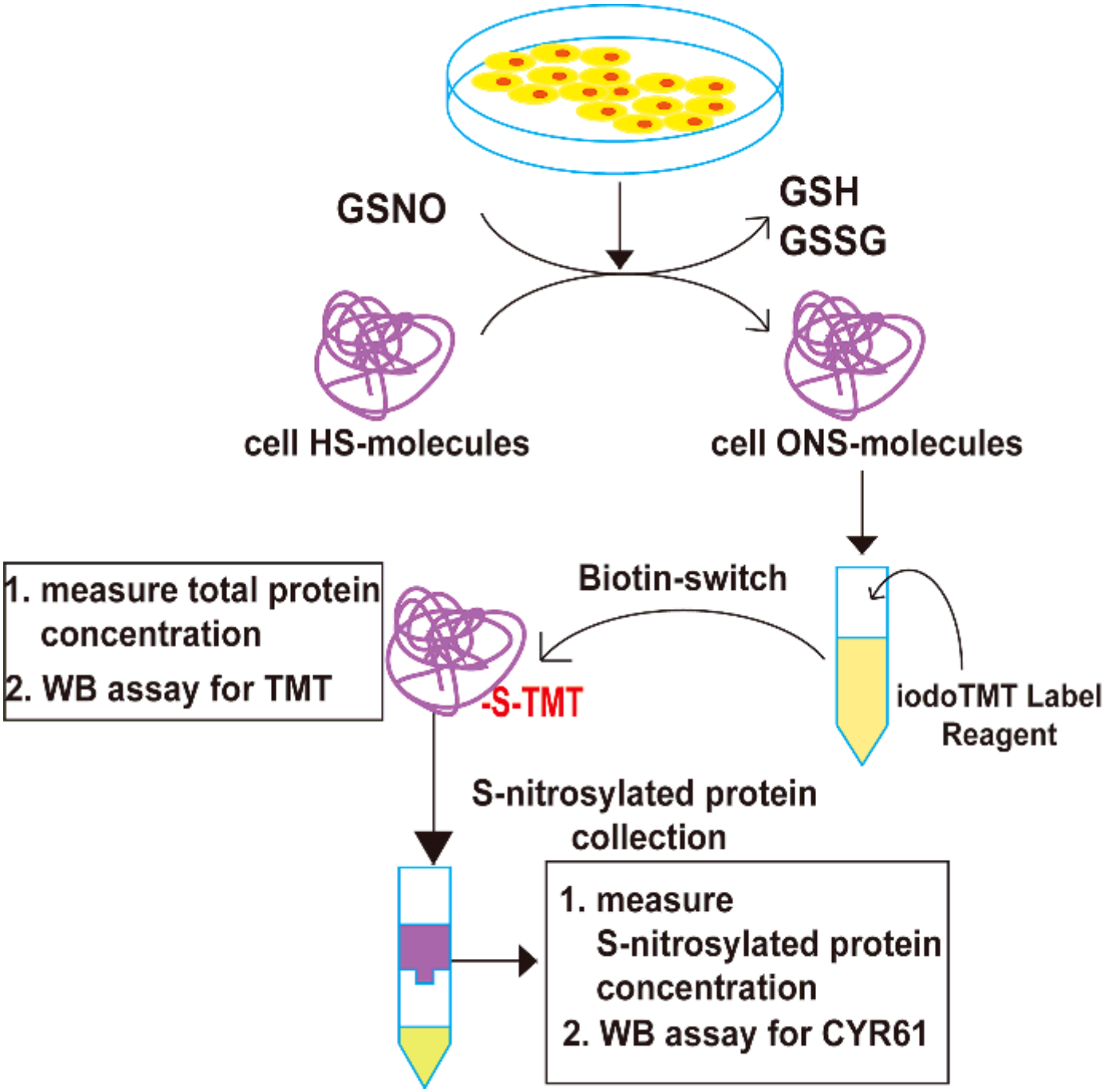

Figure 1

Workflow for quantifying S-nitrosylated CYR61 in MDA-MB-231 and its genetically-transfected cell lines. MDA-MB-231 cells and their genetically-transfected CYR61 cell lines were exposed to GSNO (10 and 30 μM) for different times to transfer cellular thiols to S-nitrosylated molecules (RSNO). The iodo TMT labeling reagent was added to the whole cell protein to transfer RSNO to RS-TMT. The total protein and its RSNO portion were measured by the BCA protein assay and the biotin-switch assay (for quantifying the S-TMT group), respectively. The RS-TMT protein was collected by the affinity resin column, and was quantitatively measured by the BCA assay. The amount of CYR61 including the RS-TMT protein was further determined by the CYR61 Western Blotting assay, and was assumed to be equivalent to that of CYR61-SNO.

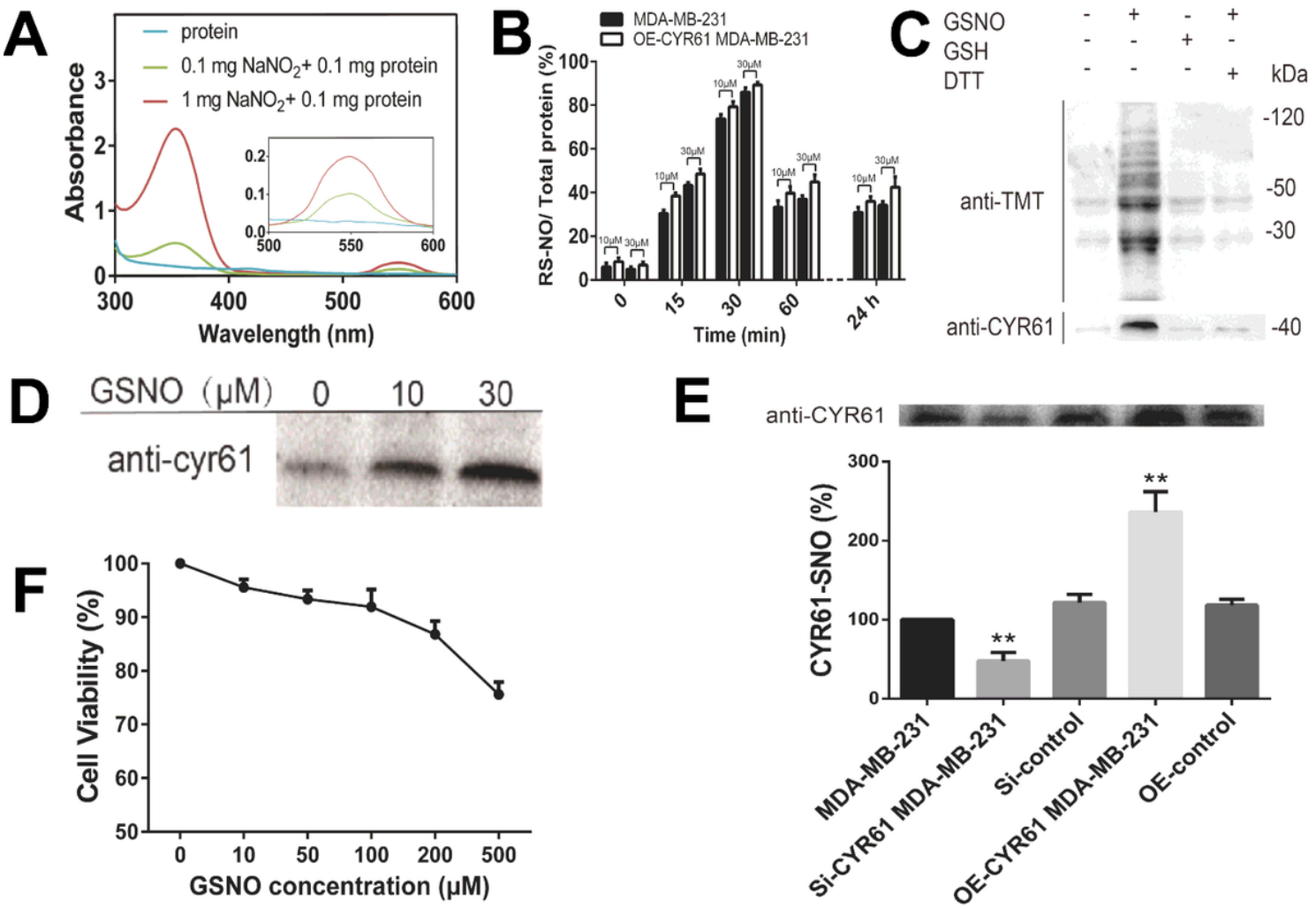

Figure 2

S-nitrosylation by GSNO of total MDA-MB-231 thiol protein, CYR61 protein and resulting cell viability. A. UV-visible spectroscopic characterization of S-nitrosylated CYR61; MDA-MB-231 lysates were treated with NO2- and then spectroscopically scanned, showing two characteristic peaks at 350 nm for nitrosation, and 540 nm for S-nitrosylation. B. S-nitrosylation dynamics of the total thiol protein (RS-NO) in MDA-MB-231 and CYR61-overexpressed MDA-MB-231 cell lines (OE-CYR61 MDA-MB-231). The S-nitrosylation was induced by GSNO (10, 30 μM) and measured by using the biotin-switch method against the total protein at assigned time points following S-nitrosylation. C. S-nitrosylation of the total protein and its proportionated CYR61 protein in MDA-MB-231 cells after 30-min treatments with GSNO, GSH, and GSNO plus DTT (all 30 μM), respectively. The proportional S-nitrosylated CYR61 was demonstrated by the biotin-switch assay and the anti-CYR61 Western Blotting analysis (the lowest panel). D. GSNO concentration-dependent CYR61 S-nitrosylation demonstrated by the biotin-switch assay and the anti-CYR61 Western Blotting analysis. E. Relative amount of S-nitrosylated CYR61 by 30 μM GSNO in MDA-MB-231 cell lines with CYR61 genetically-silenced or –overexpressed. F. Very low cytotoxicity of GSNO to MDA-MB-231 cells; at 10 and 30 μM, GSNO produced almost no toxic effect on MDA-MB-231 cells. The data represent mean± SEM (n = 3), **, P< 0.01 vs. the controls.

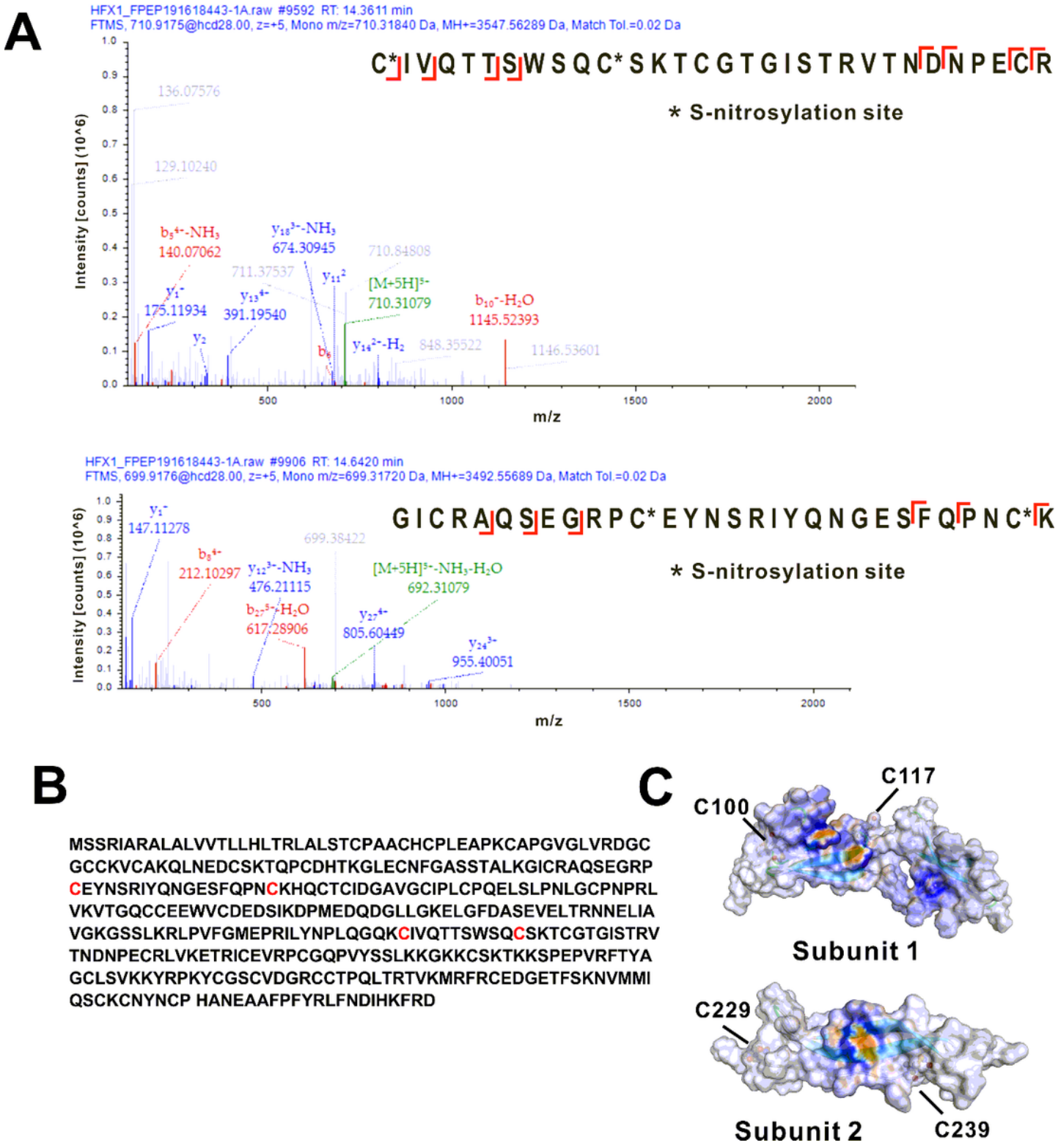

Figure 3

Proteomic and docking analyses of S-nitrosylated cysteine residues in CYR61. A. S-nitrosation of recombinant CYR61 protein was detected by using LC-MS/MS. Sequence-in-formative fragmentation ions were summarized on the peptide sequence and annotated in red (b-ions) and blue (y-ions). B. Protein sequence of human CYR61 and its S-nitrosylated sites (red-highlighted). C. The 3D structure of the CYR61

protein subunit 1 (Glu96-Asp164) and subunit 2 (Lys228-Gly273) were modeled by using MODELLER software.

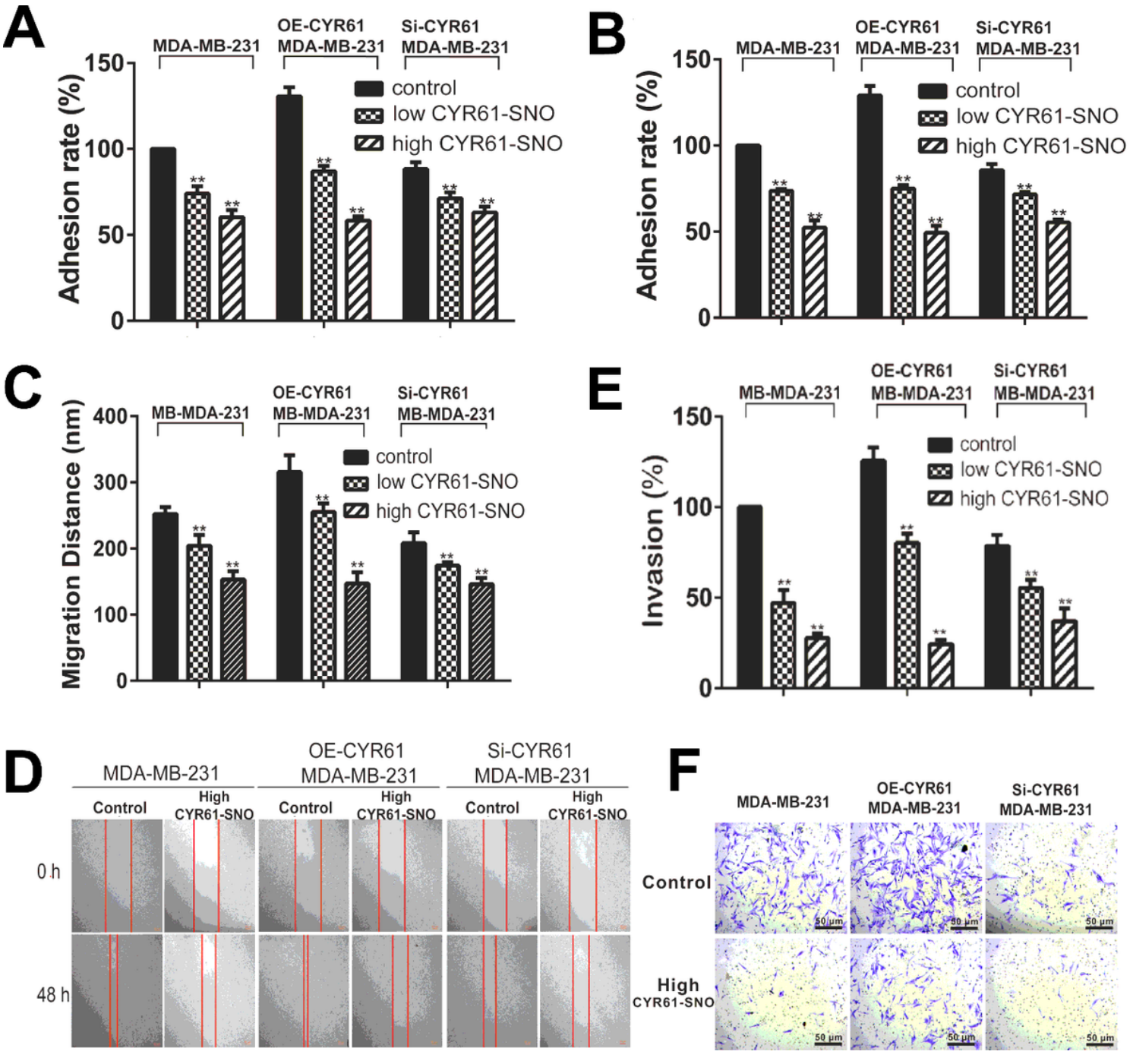

Figure 4

CYR61 S-nitrosylation inhibited adhesion, migration and invasion of MDA-MB-231 cell lines. A and B. Quantitative analysis of the effect of CYR61 S-nitrosylation by GSNO (10, 30 μM; i.e., low and high CYR61-SNO) on adhesion of the cell lines expressing high and low CYR61 (OE-CYR61 MDA-MB-231 and Si-CYR61 MDA-MB-231) to Matrigel (A) and HPMECs (B). C. Quantitative analysis of the effect of S-nitrosylation on cell migration of MDA-MB-231, OE-CYR61 MDA-MB-231 and Si-CYR61 MDA-MB-231 treated with GSNO of 10 and 30 μM (i.e., low and high CYR61-SNO) for 24 h. D. Representative images

showing that cell migration of MDA-MB-231, OE-CYR61 MDA-MB-231 and Si-CYR61 MDA-MB-231 was slowed down by S-nitrosylation. E. Quantitative analysis of the effect of S-nitrosylation on invasion of MDA-MB-231, OE-CYR61 MDA-MB-231 and Si-CYR61 MDA-MB-231 treated with GSNO (0, 10 and 30 μM) for 48 h. F. Representative images showing that the invasion ability of the tested cells was attenuated after S-nitrosylation. The data are expressed as the mean± SEM (n=3). **, P< 0.01 vs. the untreated controls.

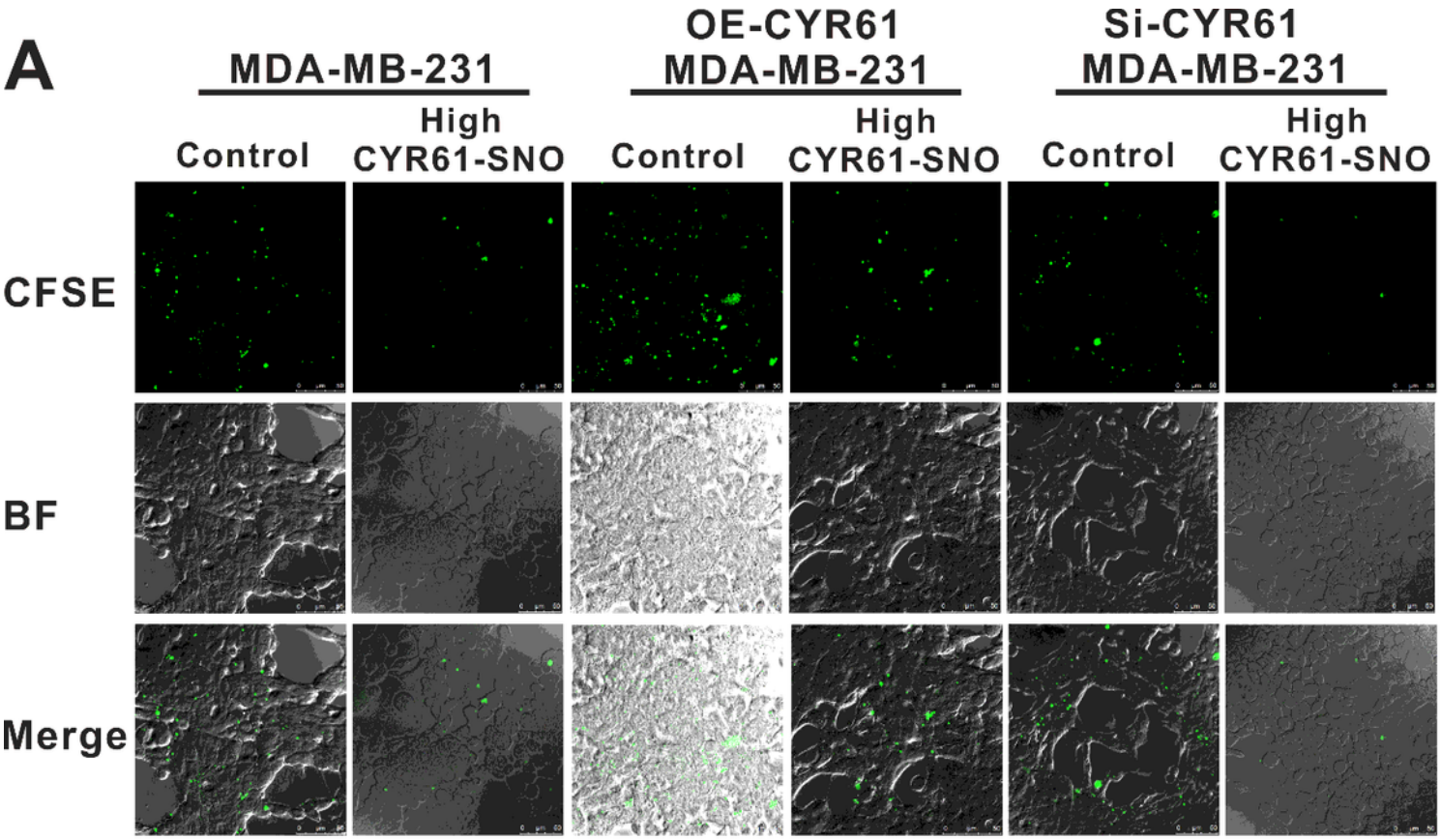

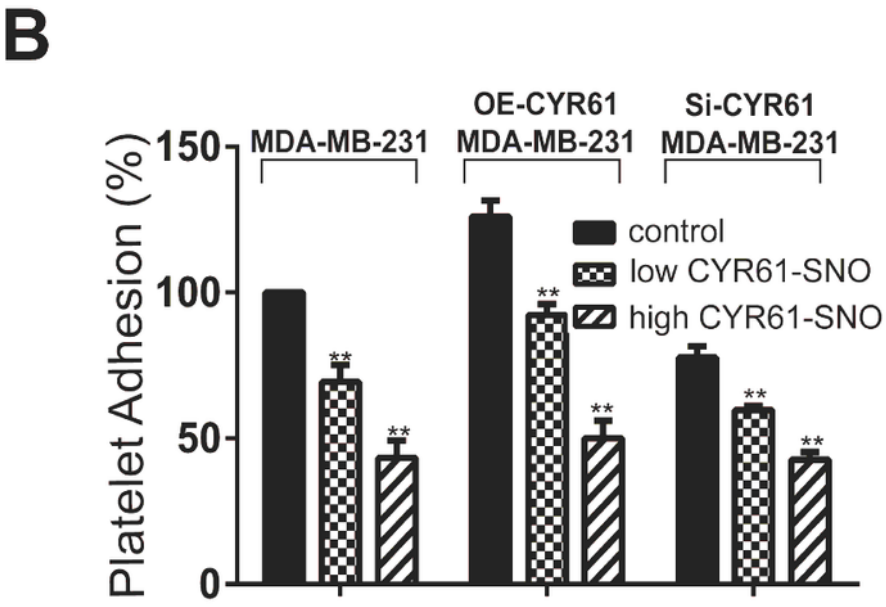

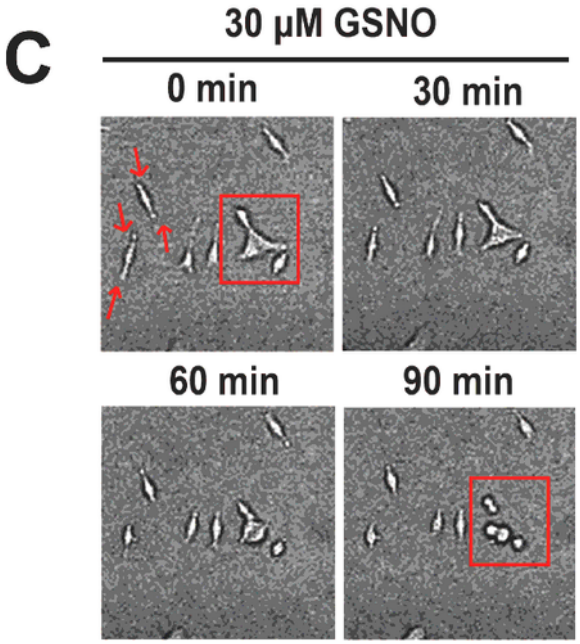

Figure 5

CYR61 S-nitrosylation inhibited adhesion between platelets and MDA-MB-231 cell lines. A. Representative images showing that adhesion between platelets and the tested cell lines was attenuated after S-nitrosylation. The upper panel showing that the CFSE-labeled platelets adhered to the tested cell lines with or without S-nitrosylation. The middle panel shows the MDA-MB-231 and their transfected cells under bright fields (BF) of fluorescence microscopy. The lower panel shows adhesion between the ADP-activated platelets and MDA-MB-231 cells, or their transfected cells after washing out all the unattached platelets. B. Quantitative analysis of the effect of S-nitrosylation on adhesion between platelets and MDA-MB-231, OE-CYR61 MDA-MB-231 and Si-CYR61 MDA-MB-231 treated with GSNO of 10 and 30 μM (i.e., low and high CYR61-SNO) for 24 h. C. Confocal microscopy images focused on the same spot to show the morphological changes of the same MDA-MB-231 cells with time after S-nitrosylation. Note, the cell body changed from spindle to more round shape (see the arrows), and the attached cells gradually became unattached after GSNO treatment (see the squares). The data are expressed as the mean± SEM (n=3). **, P< 0.01 vs. the untreated controls. The images represent five individual observations (scale bar 50 μm). CFSE, carboxyfluorescein diacetate succinimidyl ester.

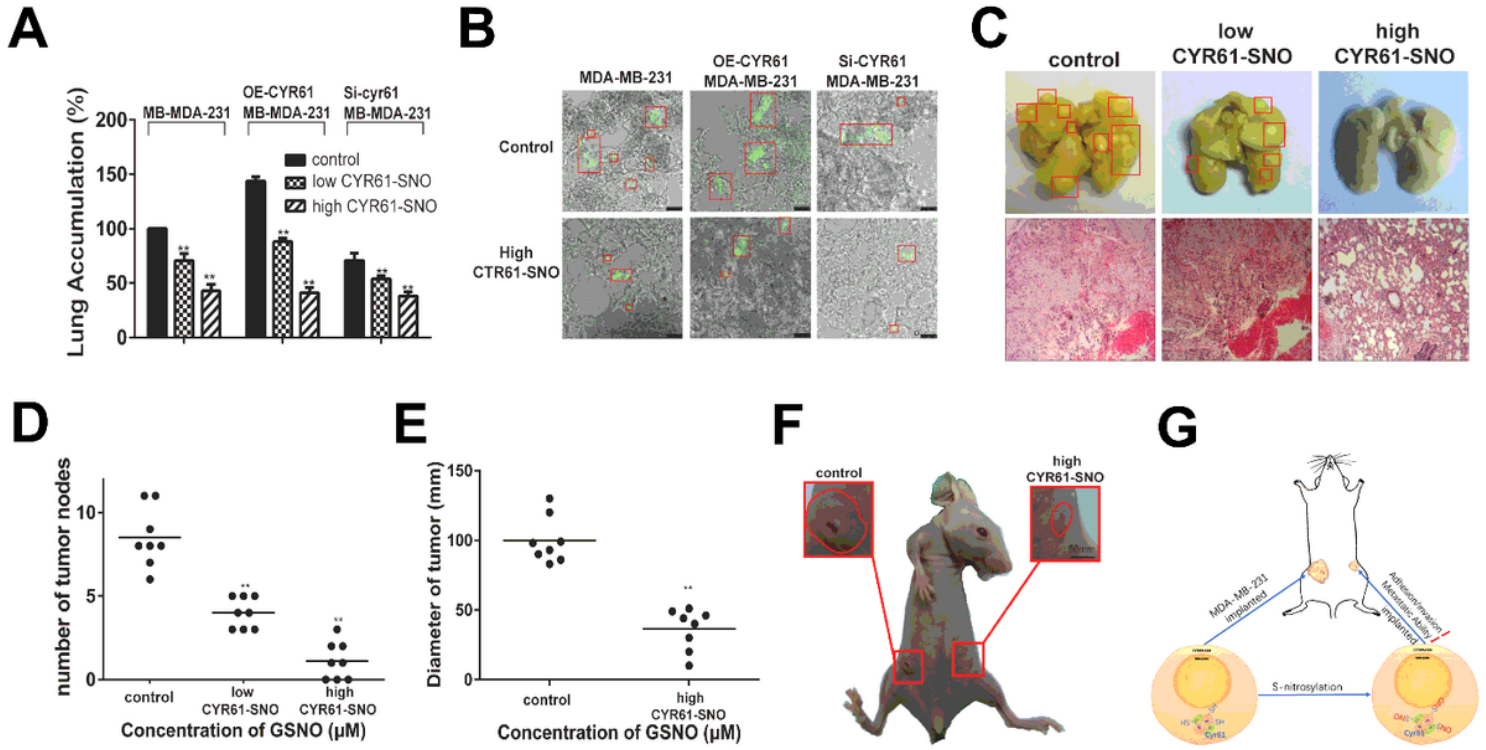

Figure 6

Effects of CYR61 S-nitrosylation on in vivo metastasis of MDA-MB-231 cell lines. A. Quantitative analysis of the acute adhesion and accumulation of three MDA-MB-231 cell lines in lungs of female BALB/C nude mice 4 hours after tail vein injections of the cells (n= 5/group). The three cell lines were pretreated with GSNO (0, 10 and 30 μM) for 30 min followed by washing the GSNO off before injections of the cells into the mice. B. Representative images of the acute lung adhesion and accumulation of the three cell lines with or without 30-min pretreatment with GSNO (30 μM). C. Photography evidence (upper panel) of mouse lung metastasis and the corresponding HE histology staining (lower panel) ten weeks after

injection of MDA-MB-231 cells with or without 30-min pretreatment with GSNO (0, 10 and 30 μM). D. Number of tumor nodes formed by MDA-MB-231 cells ten weeks after their injections via tail vein into female BALB/C nude mice (n= 8-10/group). The cells were pretreated with GSNO (0, 10 and 30 μM) for 30 min followed by washing GSNO off before cell injections. High level of S-nitrosylation significantly attenuated lung metastasis by MDA-MB-231 cells. E. Quantitative analysis of the tumor diameter of 2 weeks after injections of untreated MDA-MB-231 cells (Control) and the GSNO-treated MDA-MB-231 cells (high CYR61-SNO) to mammary fat pad. The GSNO-treated MDA-MB-231 cells resulted in no lung metastasis 6 weeks after the implantation, whereas, MDA-MB-231 cells produced the positive metastasis. F. Representative photograph shows orthotopic primary tumor formation 2 weeks after injections of MDA-MB-231 cells (left mammary fat pad) and the GSNO-treated MDA-MB-231 cells (right mammary fat pad) to the same nude mouse, respectively. Smaller tumor formation on the right mammary fat pad (n= 8/group). G. S-nitrosylation of the cysteine-rich CYR61 protein leads to attenuation of the adhesion/invasion/metastasis ability of the triple-negative breast cancer (TNBC) MDA-MB-231 cells. The data are expressed as the mean± SEM. *, P< 0.05; **, P< 0.01, and ***, P< 0.001 vs. the untreated controls.